Laminar Flow Sections for Proa Boards and Rudders

Thomas E . Speer, Des Moines, Washington, USA

ABSTRACT

Hydrofoil section designs for proa sailboats which reverse direction in a shunt when changing tacks are presented. These sections have fore-aft symmetry with blunt leading and trailing edges. The design rationale for three families of sections is discussed. XFOIL computed data are provided for all sections at Reynolds numbers of 500,000 to 2,000,000, cambers ranging from 0 to 2%, and thickness ranging from 8% to 12%

The Proa 1-series were based on circular biconvex thickness distributions with rounded edges. This series exhibited excessive drag and flow separation. The Proa 2- and 3-series were designed using an inverse method. A boundary layer trip was found to be necessary for the Proa 2 series. The Proa 3 series achieved performance comparable to NACA sections without a boundary layer trip.

NOTATION

c	chord, ft
$C_d = \frac{d}{\frac{1}{2} r V_0^2 c}$	section drag coefficient
$C_l = \frac{l}{\frac{1}{2} r V_0^2 c}$	section lift coefficient
$C_p = \frac{p - p_0}{\frac{1}{2} r V_0^2}$	pressure coefficient
d	drag per unit span, lb/ft
l	lift per unit span, lb/ft
$R_e = \frac{r V_0 c}{m}$	chord Reynolds number
p	pressure, lb/ft^2
V_0	freestream velocity, ft/sec
α	angle of attack, deg.
μ	kinematic viscosity, slug ft^2/sec
ρ	density, slug/ft^3

INTRODUCTION

Proas are multihull sailboats which have two unequal hulls. The Pacific proa variety, descended from the sailing log canoes of the Pacific islands, always keeps the same hull to windward. It changes tacks by shunting in which it stops and reverses direction rather than by turning though the wind as is done with Western sailing craft. The Pacific proa therefore has fore-aft symmetry rather than the port-starboard symmetry of other craft. Boards and rudders for shunting proas must either be rotated through nearly 180 degrees when shunting, or must reflect the fore-aft symmetry of the boat.

The latter requires an unconventional approach to section design for boards and rudders. Conventional airfoils and hydrofoils have rounded leading edges and sharp-edged trailing edges. Fore-aft symmetric sections must either have sharp leading and trailing edges or blunt leading and trailing edges. Sharp leading edges are subject to separation, ventilation and leading edge stall, but have good characteristics at the trailing edge. Blunt trailing edges have their own problems with regard to trailing edge separation and pressure drag. Rounded leading edges are capable of operating at higher lift coefficients without stalling than are sharp leading edges.

This paper adopts the blunt-edged approach to proa section design. The goal of the proa section designs was to provide performance comparable to that of conventional airfoils.

The designation for each member of the proa families was of the form "Pnrytt" where "P" designated the section as intended for proas, "n" identified the section as belonging to a given series, "r" indicated the applied leading edge radius (if any) in percent chord, "y" indicated the maximum camber in percent chord, and "tt" the thickness in percent chord. The position of maximum camber and thickness was always at mid chord due to symmetry.

All of the data were computed using Drela's XFOIL program (Drela and Youngren, 2000). XFOIL uses a

high order panel method to calculate the inviscid flow about an airfoil, coupled with an integral boundary layer method. It includes both an analysis capability and an inverse design capability. The coupled viscous-inviscid calculation is capable of handling modest amounts of separation.

The blunt trailing edge sections analyzed in this paper barely met the assumptions behind XFOIL's methodology. Therefore, the results should be treated with some caution until confirmed by experiment.

In the sections to follow, the basic flow phenomenology which drove the designs is discussed. Detailed rationale and selected performance data for three families of sections are presented. Complete data for the three families are contained in the appendices.

PHENOMENOLOGY

Figure 1 shows the pressure distribution about the NACA 65-012 airfoil at two degrees angle of attack. The dotted line shows the inviscid pressure distribution about the airfoil, computed without any boundary layer effects. The solid lines show the pressure distribution with the boundary layer included. The lower surface had a favorable pressure gradient with a decreasing pressure from the leading edge to mid chord. Both surfaces had an adverse pressure gradient over the aft half of the airfoil. The upper surface also showed the formation of a suction peak at the leading edge.

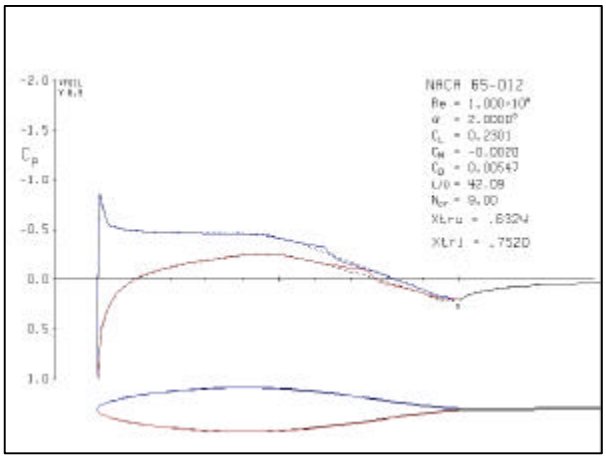

Fig. 1, NACA 65-012 at 2 Degrees Angle of Attack

The boundary layer on both surfaces was predicted to be laminar from the leading edge to part way down the adverse pressure gradient. Laminar separation occurred at approximately 55% chord on the upper surface and 62% chord on the lower surface. In both cases, the flow transitioned from laminar to turbulent and reattached, forming a laminar separation bubble. This is evidenced on the diagram by the bumps in the pressure distribution on each surface.

The structure of a laminar separation bubble is shown schematically in Figure 2. An adverse pressure gradient causes the laminar boundary layer to separate. When it separates, the free shear layer is free to move in response to pressure changes, so the pressure becomes approximately constant. The separated laminar flow is highly unstable, however, so it rapidly transitions to turbulent flow.

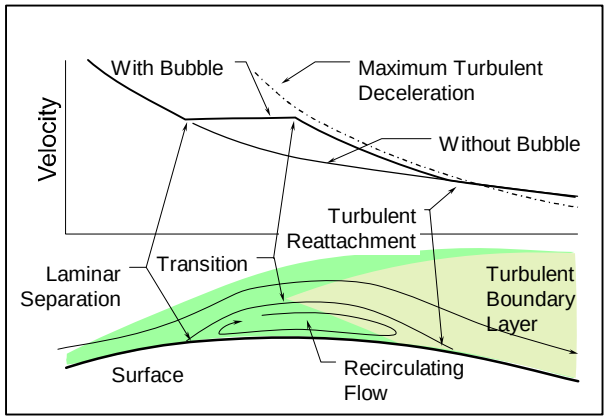

Fig. 2, Laminar Separation Bubble

Once transition occurs, the pressure begins to increase a very nearly the maximum rate which can be sustained by the turbulent boundary layer. If the turbulent deceleration profile intersects the inviscid pressure distribution, the flow reattaches. The dividing streamline running between the separation and reattachment points separates the flow into two regions: the flow passing by the separation bubble and a region of recirculating flow within the bubble

If the two curves do not intersect, the flow remains separated and the section stalls. Thus the nature of the flow can change rapidly when the slope inviscid pressure distribution increases, as it does with an increase in angle of attack. The change in slope with angle of attack can be seen by comparing the pressure distributions of this symmetrical section, as the top surface distribution represents a change of four degrees angle of attack from that of the bottom surface.

In addition to laminar separation and turbulent reattachment, at the Reynolds numbers considered, the flow can also transition to turbulent through amplification of disturbances in the boundary layer. Adverse pressure gradients increase this amplification and thus the location of this type of transition can also be controlled through design of the pressure distribution.

Finally, the displacement thickness of the boundary layer is depicted on the plot of the airfoil shape beneath the pressure distribution. The thin trailing edge of the NACA 65-012 allows the attached boundary layer to smoothly leave the airfoil, resulting in a thin, low-drag

wake. The wake is much thicker behind the blunt-edged proa sections presented below.

PROA 1-SERIES

The first series considered was intended to be representative of the type of sections used for fore-aft symmetrical proa hydrofoils. The Proa 1-series used a geometrical construction shown in Figure 2. It consisted of a symmetrical thickness distribution formed by two circular arcs of large radius and a leading edge radius tangent to the ogival body at each end. The thickness distribution was combined with an NACA a=1 camber line. This camber provided a uniform load over the section chord at zero angle of attack and maintained the fore-aft symmetry. The leading edge radius used in the P11ytt sections was 0.75% chord and the leading edge radius for the P12ytt sections was 1.5% chord.

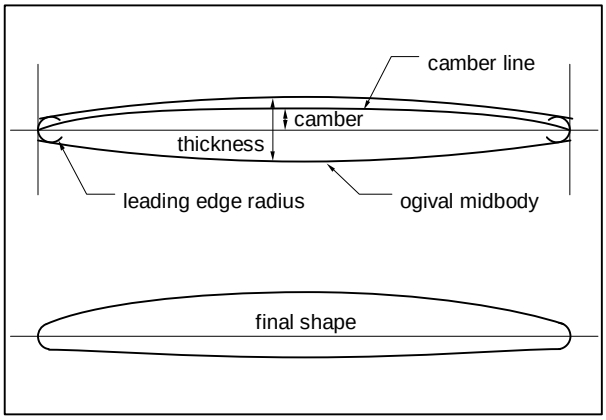

Fig. 2, Proa 1-Series Construction

The pressure distribution about the P12212 section at one degree angle of attack is shown in Figure 3. This distribution was typical of the sections in this family. A pronounced pressure peak existed at the leading edge on both sides. The steep adverse pressure gradient associated with the peak caused laminar separation and the formation of a separation bubble immediately behind the leading edge. As a result, the boundary layer along the entire surface was turbulent.

The best performance of the Proa 1-series sections is shown in Figure 4. The performance of the NACA 0012 is also shown for comparison. The leading edge separation of the Proa-1 series severely limited the ability of XFOIL to calculate the performance. Converged solutions were only obtained for a narrow range of angles of attack. This range did not provide a useable range of lift coefficients. The drag was also twice as high as that of the NACA 0012. As a result, the Proa 1-series was not considered to be an acceptable design.

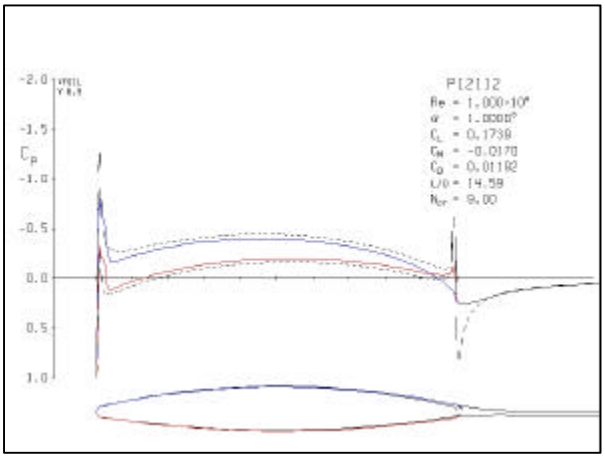

Fig. 3, P12212 Pressure Distribution

Proas currently in service so not appear to suffer as extensively from these problems as indicated by these data. It may be possible that the leading edge separation that occurs in practice is not as severe as predicted by XFOIL. Nevertheless, it appeared that the geometric approach to section design for proas was not promising.

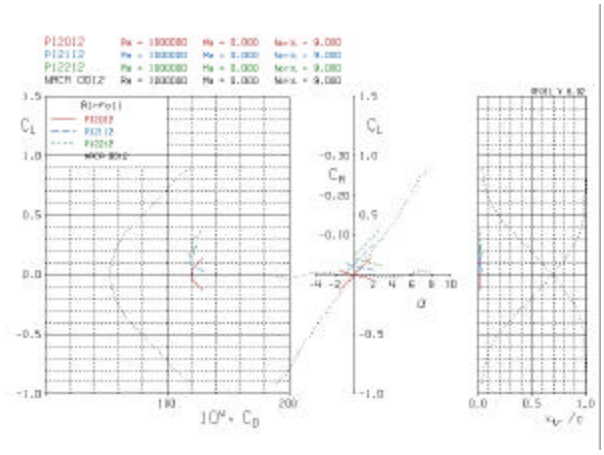

Fig. 4, Proa 1-Series Performance

PROA 2-SERIES

A modern inverse design approach was adopted for the subsequent series of section designs. These were designed by specifying symmetrical inviscid pressure distributions at zero angle of attack and using XFOIL to calculate the required shape. The shapes were refined to ensure perfect symmetry and analyzed for performance. No modification of the edges was done to impose a given leading edge radius, so the designations for the Proa 2-series were all of the form "P20ytt" with "y" and "tt" indicating the camber and thickness in percent chord as before.

Figure 5 shows the design pressure distribution for the P20208 section, which was the archetype for the second series. The design pressure was essentially flat acrosss the entire chord on both surfaces. The P20208 lower surface velocity was very close to freestream and the near uniform loading resulted in a camber line similar to that of the NACA a=1 camber line.

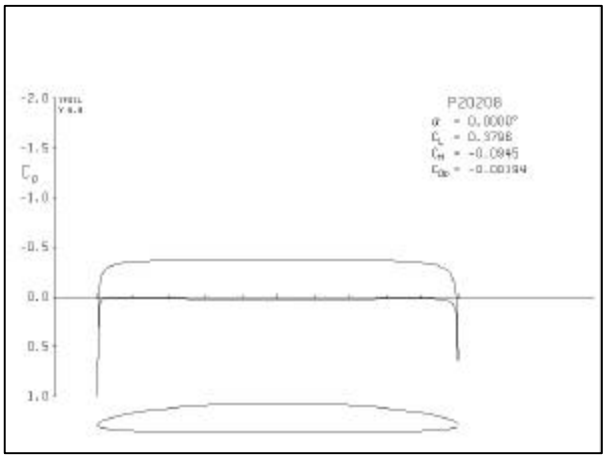

Fig. 5, P20208 Design Pressure Distribution

The viscous pressure distribution at chord Reynolds number of 1,000,000 for is shown in Figure 6. The inviscid pressure distribution from Figure 5 is shown by the dotted line. The flow on the lower surface was laminar and attached until immediately ahead of the trailing edge. The upper surface was laminar and attached to approximately 92% chord, where it separated. The flow transitioned to turbulent just ahead of the trailing edge, followed by a steep increase in pressure.

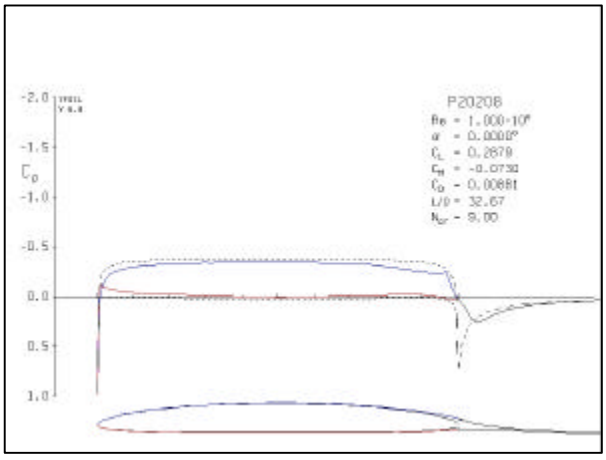

Fig. 6, P20208 Pressure Distribution, a = 0

The separated flow on the upper surface trailing edge resulted in a thicker boundary layer there, as can be seen by the displacement thickness plot. This reduced the effective camber at the trailing edge and reduced the circulation about the section. The reduced circulation affeced the leading edge in much the same manner as a reduction in angle of attack. This is shown in Figure 7, which presents the inviscid pressure distribution for the same lift coefficient as Figure 6. The increase in velocity on the lower surface leading edge is clearly evident. The effect is larger than the viscous case because for the inviscid pressure distribution nearly all of the change in lift occurs at the leading edge, whereas in the viscous case much of the difference is at the trailing edge, too. So a better match could be obtained with an intermediate angle of attack. However, the two cases presented illustrate the effect of viscous coupling of the flow at the trailing edge with the flow all around the section.

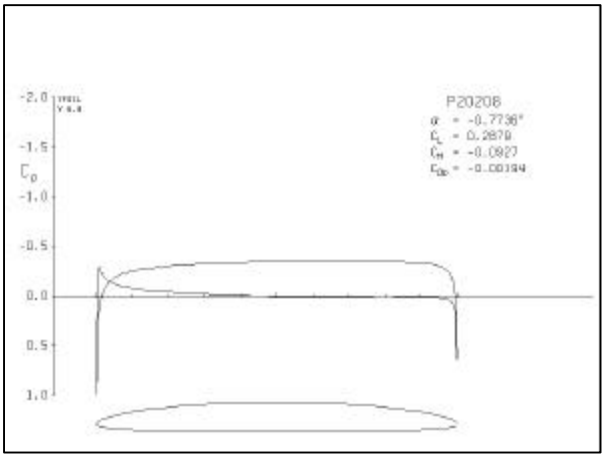

Fig. 7, P20208 Pressure Distribution, C_l=0.29

The other members of the Proa 2-series were constructed by varying the thickness and camber from the P20208 section. Figures 8 and 9 show the design pressure distributions for two other members of the family. The essential character of the flat pressure distributions was retained with changes in camber and thickness. Thickness raised the velocities on both surfaces, while camber increased the difference between the velocities on each surface.

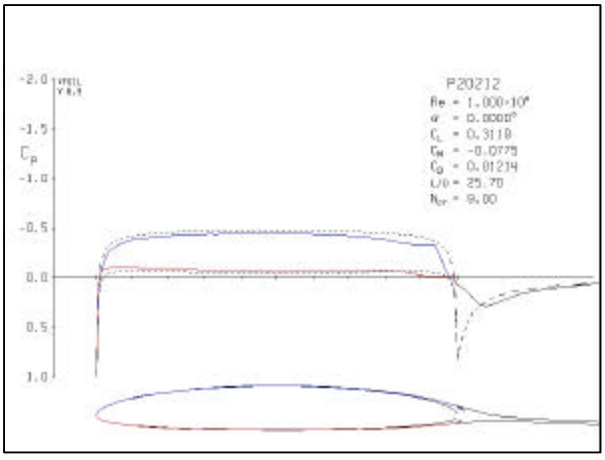

Fig. 8, P20212 Design Pressure Distribution

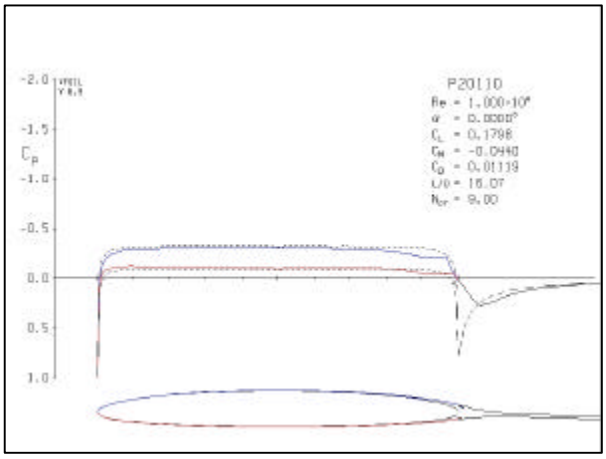

Fig. 9, P20110 Design Pressure Distribution

The performance of these Proa 2-series sections is shown in Figures 10 to 13. (See appendices for the same data presented in a larger format.) The lift and moment curves (center plot in each figure) showed sudden jumps in magnitude and slope with changes in angle of attack. These jumps were correlated with sudden changes in the transition location, as can be seen in the right-hand plot of each figure. XFOIL also had difficulty with numerical convergence at these points.

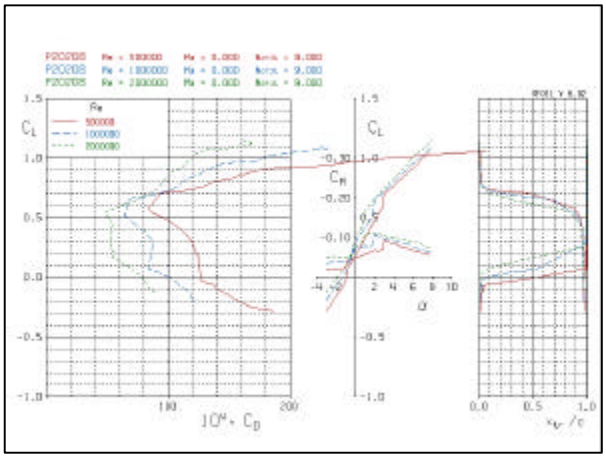

Fig. 10, P20208 Performance, Natural Transition

Five different types of flow were possible at the trailing edge: attached laminar flow, separated laminar flow, separated laminar flow with transition to turbulent, attached turbulent boundary layer, and separated turbulent boundary layer. Each surface could exist in one of these states, for a combination of twenty-five distinct flow situations at the trailing edge. The conditions at the trailing edge were not unique, but depended upon what type of flow previously existed. This is shown in Figure 13, in which the Re=2,000,000 case was swept from negative angle of attack to positive and back to negative. Near zero lift, two different values of drag were obtained as well as two different transition locations on the lower surface.

In general, the performance (left plot in each figure) was much better than the Proa 1- series, with a wider range of angles of attack and lower drag for some lift coefficients. However, the erratic nature of the aerodynamic characteristics was not acceptable.

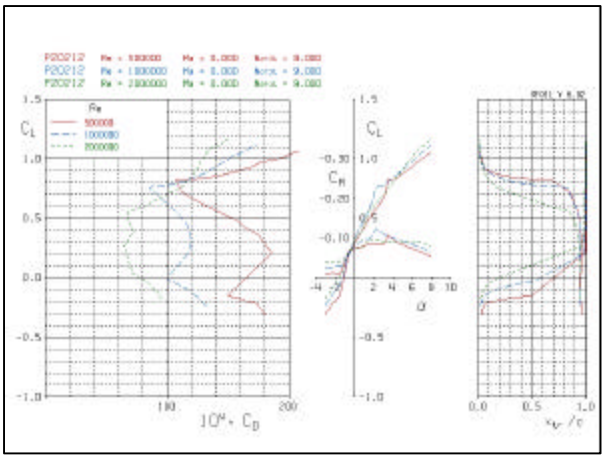

Fig. 11, P20212 Performance, Natural Transition

The five different flow types at the trailing edge was reduced to two - attached and separated turbulent flow - by the addition of a turbulator to fix transition at 50% chord. Mid chord was as far aft as the turbulator could be mounted because of symmetry.

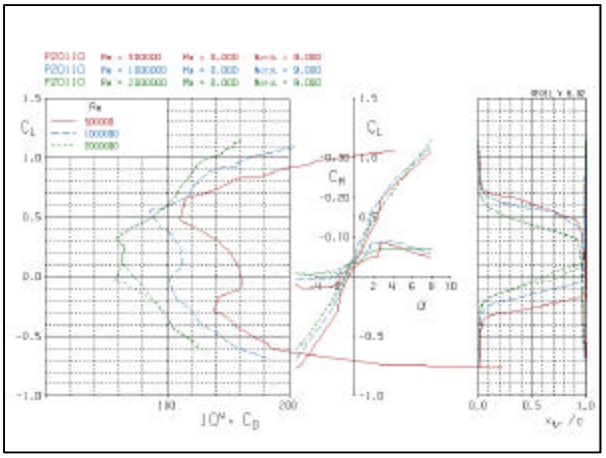

Fig. 13, P20110 Performance, Natural Transition

The performance of the three sections with fixed transition is shown in Figures 14 through 16. Fixing the transition completely eliminated the sudden jumps in lift and pitching moment. Drag was reduced for most of the low lift range. Outside of this range, the transition was triggered by laminar separation at the leading edge pressure peak and the drag increased, forming a distinct drag bucket characteristic in the drag polars.

Fixed transition also made the variations between family members of the series predictable as well. For example, Figure 17 shows the effect of varying the

camber while holding thickness constant. As expected, the aerodynamic characteristics were simply shifted to higher lift coefficients and lower angles of attack. The minimum drag and the width of the drag buckets were unchanged.

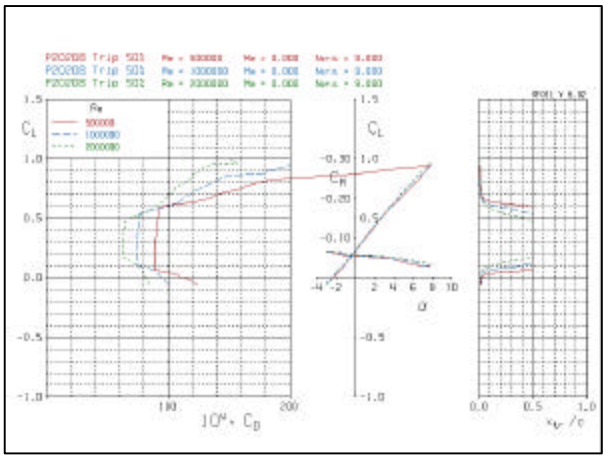

Fig. 14, P20208 Performance, Fixed Transition

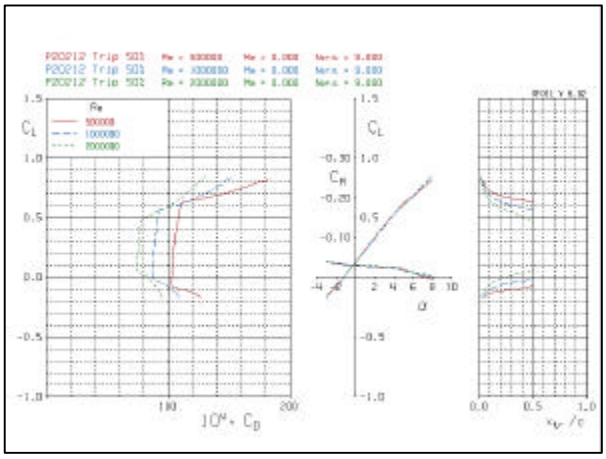

Fig. 15, P20212 Performance, Fixed Transition

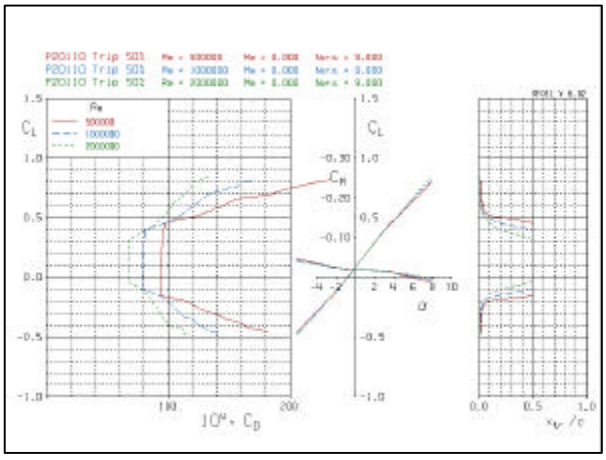

Fig. 16, P20110 Performance, Fixed Transition

The Proa 2-series with fixed transition provided useable designs. However, as seen by the comparison of selected sections in Figure 18, the series did not meet the goal of providing performance comparable to that of conventional airfoil sections, although the maximum sectional lift/drag ratio was close. Further improvement was warranted to reduce the minimum drag.

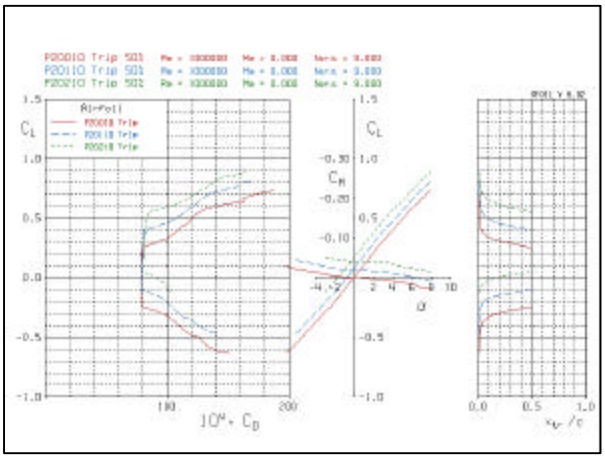

Fig 17, Proa 2-Series Effect of Camber

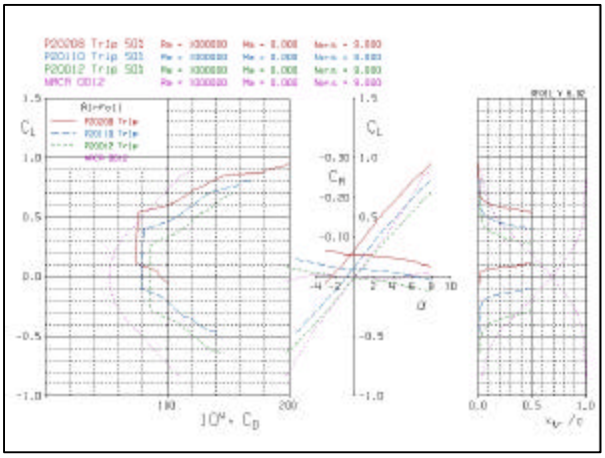

Fig. 18, Proa 2-Series vs. NACA 0012

PROA 3-SERIES

The Proa 2-series showed the importance of ensuring transition occurred well ahead of the trailing edge. For the Proa 3-series, the design pressure distribution was given a peaked-roof shape, with an adverse gradient running from mid chord to the trailing edge, as shown in Figure 19. The velocity was increased at the leading and trailing edges on the lower surface. This increased the camber at the ends and made the edges thinner. It also promoted attached flow on the lower surface trailing edge. At the design condition, the flow on the upper surface transitioned at approximately 90% chord, while the lower surface was fully laminar and attached all the way to the trailing edge.

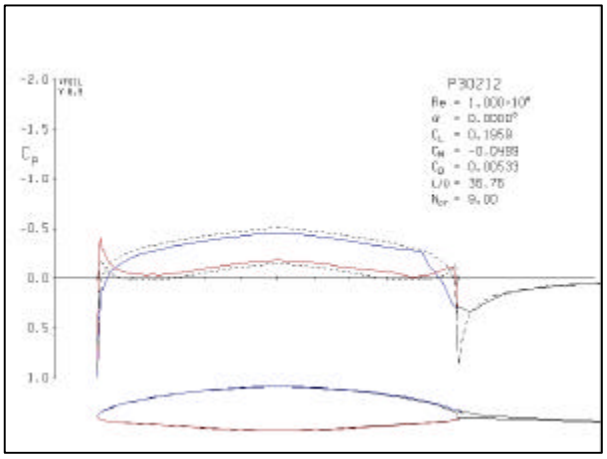

Fig. 19, P30212 Design Pressure Distribution

This flow picture changed considerably with angle of attack, as seen in Figure 20. At an angle of attack of 2.8 degrees, the favorable pressure gradient on the forward half of the upper surface all but flattened out and a pressure peak formed at the leading edge. The transition point moved to 68% on the upper surface and the turbulent boundary layer remained attached to the trailing edge. In this case, the conditions at the trailing edge caused the lift to be slightly greater than for the inviscid case, indicating that the effects of the boundary layer did not always decrease the lift. Further increases in angle of attack amplified the leading edge pressure peak and resulted in an adverse pressure gradient over the entire upper surface.

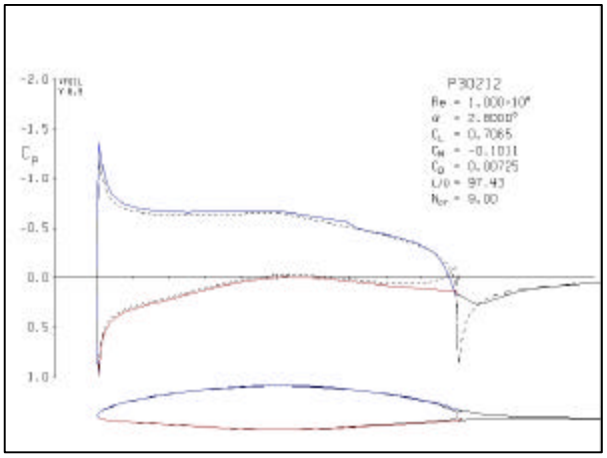

Fig. 20, P30212 Pressure Distribution, a=2.8 deg.

The performance of this section is presented in Figure 21. At Reynolds numbers of 1,000,000 and above, the drag was significantly reduced compared to the Proa 2-series. Although an increase in drag occurred in the middle lift range at a Reynolds number of 500,000, there was no significant evidence of hysteresis (see Re=500,000 and 1,000,000 traces). The transition point generally moved smoothly between the trailing edge and mid-chord as the adverse pressure gradient on the aft portion steepened with angle of attack. As with the Proa 2-series, the transition point moved rapidly from mid-chord when the leading edge pressure peak became too abrupt to maintain laminar flow.

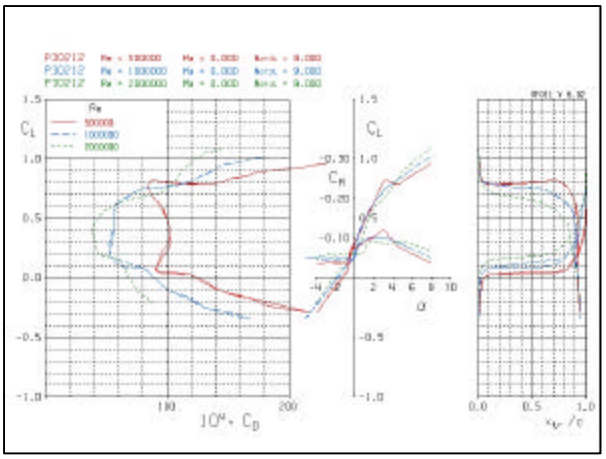

Fig. 21, P30212 Performance, Natural Transition

Adding a boundary layer trip did not benefit the Proa 3-series the same way it did with the Proa 2-series (Figure 22). The linearity of the lift and moment curves was improved, however the minimum drag was increased. Thinner versions of the Proa 3-series did not have as strong an adverse pressure gradient at the design conditions. Their characteristics were more midway between the thicker Proa 3-series and the Proa 2-series. As a result, turbulators may be more beneficial to the thinner members of the family.

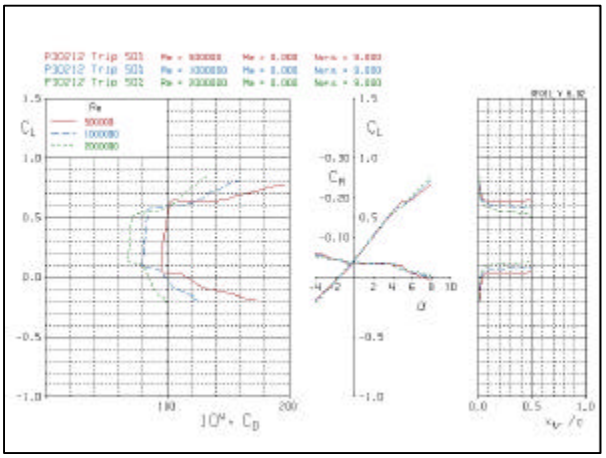

Fig. 22, P30212 Performance, Fixed Transition

Finally, the performance of selected Proa 3-series sections is compared with the NACA 0012 and NACA 65-012 sections in Figure 23. At a chord Reynolds number of 1,000,000, the minimum drag of the Proa and NACA foils was within a few counts of each other. The width of the drag bucket for the Proa foils was the same as for the NACA 65-012 laminar flow airfoil.

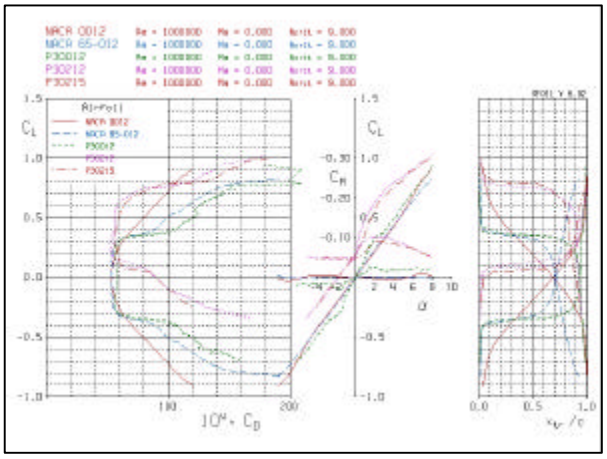

Fig. 23, Proa 3-Series Section Comparison

MOMENTS

In addition to lift and drag, the moment on the section is also important, especially with regard to the balance of a rudder. Figures 24 and 25 show the lift and moment coefficients versus angle of attack for three selected sections at a Reynolds number of 1,000,000. The P20212 (fixed transition) and P30212 (natural transition) sections have the same maximum thickness and maximum camber, while the P30012 section has the same maximum thickness but no camber. Each section has a different zero lift angle of attack, different moment at zero lift and different degree of nonlinearity to the curves.

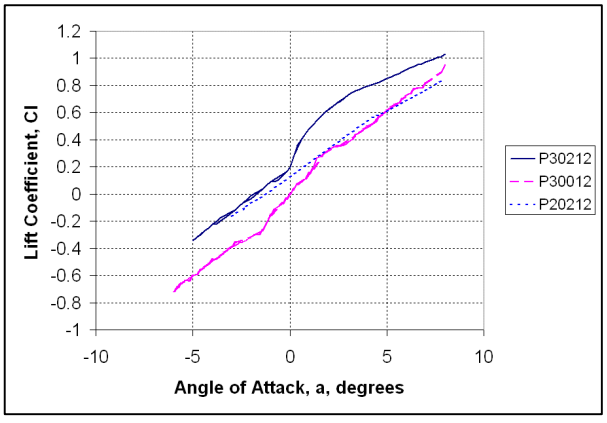

Fig. 24, Lift Curves, Re=1,000,000

The moments in Figure 25 were taken about the quarter-chord location. The positive slope of the P20212 section indicates that the hydrodynamic center is ahead of the quarter chord, while the negative slope of the P30012 section indicates its hydrodynamic center is behind the quarter chord. For the P30212 section, the hydrodynamic center is at the quarter chord for negative angles of attack, but moves strongly aft and then forward with positive angle of attack.

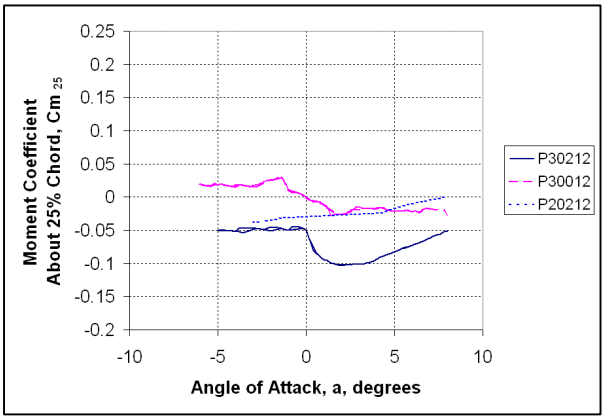

Fig. 25, 25% Chord Moment Curves, Re=1,000,000

The placement of the pivot point for a proa spade rudder that obeyed the fore-aft symmetry constraint would be at the middle of the rudder. Figure 26 shows the quarter-chord moment coefficients of Figure 25 plotted versus the lift coefficients of Figure 24. The distance, in fraction of the chord, between the hydrodynamic center and the moment reference center is equal to the slope of the curves in this plot. Overlaid on the plot are the moment coefficients corrected so as to be taken about the mid chord. Shifting the moment reference center changed the slope of the moment curves, while leaving the value of the moment at zero lift unchanged.

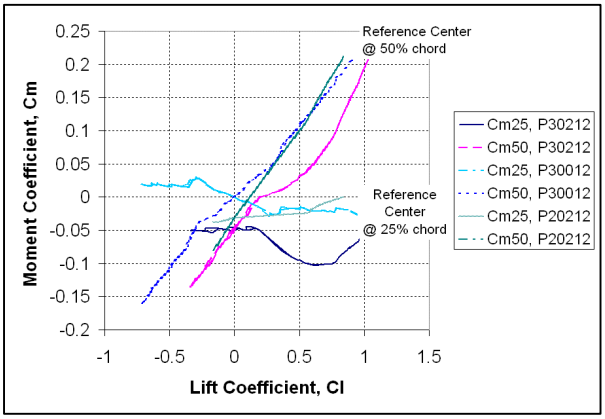

Fig. 26, Moment Coefficient vs. Lift Coefficient

Plotting the moment coefficients taken about mid chord versus angle of attack produce the remarkable result shown in Figure 27. All of the sections mid chord moments fall on the same, highly linear, line. That all of the sections had zero moment about the mid chord at zero angle of attack is a consequence of the fore-aft symmetry of the design moment curves. The highly linear nature of the moment, despite the nonlinearities in the basic lift curve and quarter chord moments, was unexpected.

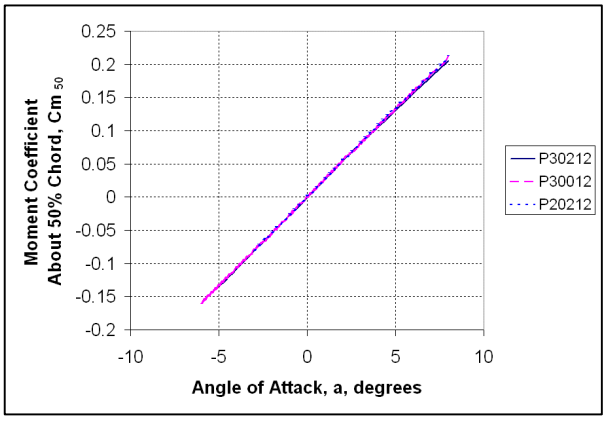

Fig. 27, 50% Chord Moment Curves, Re=1,000,000

The positive slope of the moments taken about mid chord indicated a strongly unstable moment characteristic and would make such a rudder highly over-balanced. This unstable moment makes shunting proa rudder design highly problematic. Any section design which seeks to maintain attached flow for efficiency will have this characteristic. This leaves the designer with few options.

One option is to place the pivot point toward one edge, at or ahead of the hydrodynamic center. This results in a surface which is stable when traveling in one direction and even more highly unstable when traveling in the opposite direction. When traveling in the unstable direction, the surface might be firmly fixed in position and act as the keel. A second surface, with the pivot towards the other end, would then serve as the rudder. The two surfaces would exchange roles for the opposite tack. This requires that the surfaces and their linkages have very high torsional stiffness and strength.

A second option is to place the pivot ahead of the hydrodynamic center for stability and rotate the rudder 180 degrees when shunting. In this case, there is no advantage to using the fore-aft symmetric sections developed in this paper, and a conventional symmetrical (zero camber) section with a sharp trailing edge can provide better performance.

CONCLUSIONS

The goal of producing fore-aft symmetric blunt edged foils with comparable performance to conventional NACA foils was met. The Proa 3-series foils have adequate performance over a useful range of angles of attack and Reynolds numbers, and can be used without a turbulator.

The Proa 2-series sections were useable, provided a turbulator was added at 50% chord on both surfaces. The Proa 3-series had lower drag, so there was little reason to use the Proa 2-series sections. However, they are worth investigating experimentally to determine whether these predictions are accurate.

The geometric construction approach of the Proa 1-series did not yield useful sections. XFOIL was unable to compute the flow outside of a very narrow range of angles of attack because of the pronounced pressure peaks generated at the intersection of the leading edge radius and the mid-body contours.

Placing the pivot point of a proa rudder at mid chord so as to respect the fore-aft symmetry of the boat results in a highly unstable, unbalanced surface. Satisfactory balance in the rudder may be obtained by using a separate rudder surface optimized for each tack, or a conventional section which is rotated 180 degrees when shunting.

XFOIL proved to be a useful tool for designing and analyzing fore-aft symmetric blunt-edged sections.

Experimental data collected in a wind tunnel or tow tank would be very valuable to verify the predictions for these sections.

REFERENCES

Abbott, Ira H., and Von Doenhoff, Albert E., "Theory of Wing Sections," Dover Publications, New York, USA, 1959.

Drela, Mark and Youngren, Harold, "XFOIL User's Manual," http://raphael.mit.edu/xfoil/, 2000.

Eppler, Richard and Somers, Dan, "Airfoil Design for Reynolds Numbers Between 50,000 and 500,000," (publisher unknown), ~1986.

van Ingen, J. L, and Boermans, L. M. M, "Aerodynamics at Low Reynolds Numbers: A Review of Theoretical and Experimental Research at Delft University of Technology," (publisher unknown), ~ 1987.